A THYRATRON-BASED PULSE GENERATOR FOR FUNDAMENTAL STUDIES OF NO_x REMOVAL IN NONTHERMAL PLASMAS

R.A. Korzekwa and L.A Rosocha
Los Alamos National Laboratory

INTRODUCTION

Nonthermal plasmas, generated by electric discharges and electron beams, have previously been used in the investigation of NO_x removal as well as the removal of other unwanted pollutants [1-5]. Although most pulsed corona discharges are driven by relatively fast risetime pulse generators (typically 10 ns or greater), most dielectric-barrier discharges have been driven with low frequency (a few to tens of kilohertz) ac power circuits or inverters. For a given gap spacing in dielectric barrier cell, the breakdown voltage of a cell driven by a fast pulse generator can be several times higher than that of a low frequency driven cell. A fast-risetime thyratron switched pulse generator circuit and dielectric-barrier discharge cell has been developed to investigate the effect on NO_x reduction of the higher breakdown voltage and resulting reduced electric field strength, E/N, at breakdown. This fast pulsed nonthermal plasma generator was also designed to provide a low temporal and spacial jitter for the investigation of the plasma chemistry properties by laser induced fluorescence (LIF) and tunable diode laser absorption spectroscopy (TDLAS). The initial results presented here include 1) a comparison of the removal efficiency of NO in nitrogen between the pulsed dielectric-barrier discharge and a pulsed corona discharge and, as another point of reference, 2) a comparison of the removal efficiency of an example chlorinated hydrocarbon trichloroethylene (TCE), in dry air between the pulsed dielectric-barrier discharge and an ac-driven dielectric-barrier discharge.

EXPERIMENTAL SETUP

Pulse Generator

A low power, high-voltage pulse generator capable of driving a small dielectric-barrier discharge cell was designed to meet specifications for low temporal jitter required by plasma chemistry diagnostic systems, such as LIF [6]. Figure 1 shows a schematic diagram of the high-voltage pulse generating circuit. To

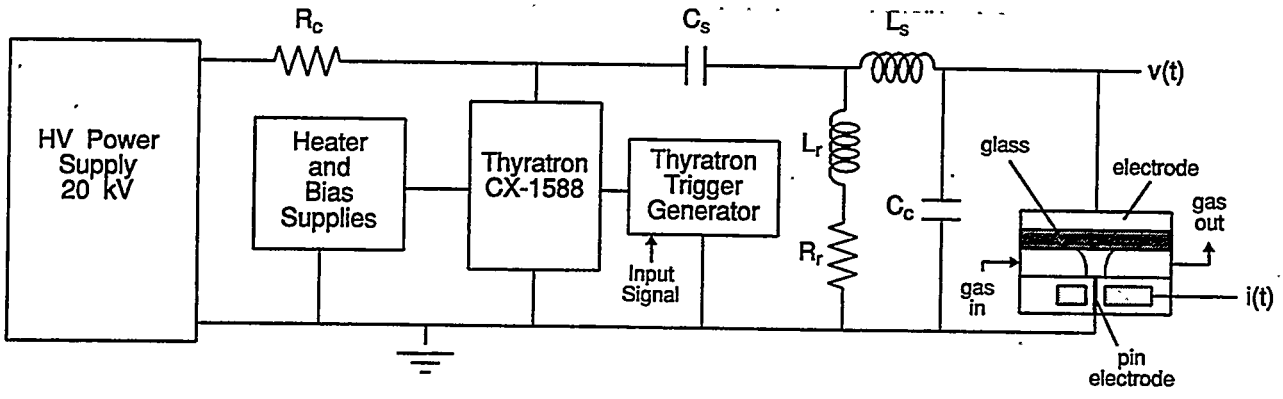

Figure 1. The thyratron-based high-voltage pulse circuit with dielectric-barrier discharge cell.

obtain a temporal jitter of less than 5 ns, a commercially available fast-risetime hydrogen thyratron tube (CX-1588, EEV Inc.) was used to switch the high-voltage pulse circuit. This low pressure hydrogen thyratron tetrode requires heater supplies for both the cathode and the hydrogen reservoir as well as bias supplies for the two grids. A positive bias voltage (50 V), with a current limiting resistor, creates a low current discharge between grid1 and the cathode. A negative bias voltage (-100 V) was supplied to the grid2 with respect to the cathode to prevent triode firing of the tube. A trigger generator (Northstar Research Corp., Model TT-18-V) was capacitively coupled to grid2 to trigger the thyratron. A low voltage pulse (5V peak with a <10 ns risetime) was used as the input to the trigger generator. A positive 20 kV dc high-voltage power supply (Plastic Capacitors, Inc., Model HV200-152M) was used to charge a storage capacitor, C_s, through a current limiting resistor, R_c = 25 MW. the slow charging process, the "ringout" inductance, L_r = 3 mH, and resistance, R_r = 50 W, effectively grounds the other side of C_s. The thyratron tube was used to switch the positively charged storage capacitor to ground which produces a negative pulse across L_r, R_r and the rest of the circuit. The risetime of the high-voltage pulse produced at the cell is set by the series resonant frequency of the combination of C_s, the stray inductance (L_s), and the high-voltage output cable capacitance (C_c). For proper circuit operation, the conditions $L_r >> L_s$ and C_c much greater than the cell capacitance must be met. In this case, C_s = 1.2 nF, L_s = 90 nH, and C_c = 150 pF (150 cm of RG-217 coaxial cable) which gives a risetime of 6.5 ns. The maximum cell capacitance without a discharge was approximately 15 pF. For a series resonant circuit, when $C_s >> C_c$ the peak voltage produced at the cell is a factor of two greater than the initial voltage on C_s. Therefore, for this pulse generator, the peak voltage is variable up to 40 kV. The dielectric-barrier discharge occurs on the risetime of the output voltage pulse. After the discharge occurs, the low frequency resonant circuit composed primarily of C_s, L_r and R_r slowly "rings out" and dissipates the remaining energy stored in the circuit in R_r so that another charge/-discharge cycle can be initiated after an appropriate delay set by the desired repetition frequency. The repetition frequency for this configuration is limited to 20 Hz. The maximum temporal jitter between the trigger input signal and the initiation of the dielectric-barrier discharge was 4 ns.

Voltage and current diagnostics were used to measure the associated waveforms which provide a measurement of the energy dissipated in the discharge plasma. The voltage, V(t), was measured using a high-voltage probe (Tektronix, model P6015A) and the current I(t) is measured using a current probe (Pearson, model 2877) as seen in Fig. 1. Both probes were calibrated before use to ensure accuracy at these frequencies and to ensure that the delays of the signal cables from the probes to the oscilloscope were equal. Typical voltage and current waveforms are shown in Fig. 2.

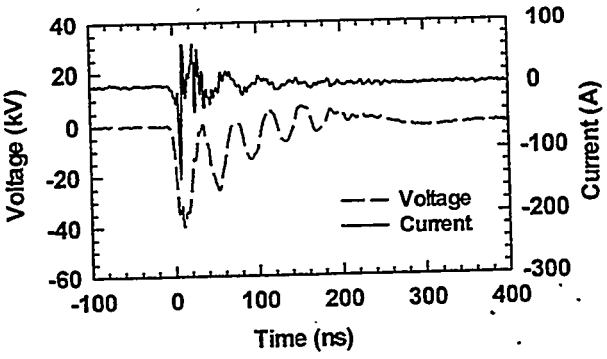

Figure 2. Typical voltage and current versus time waveforms produced at the dielectric-barrier discharge cell.

The series resonant charging of C_c is seen in the voltage waveform and is associated with the high-frequency oscillation. A lower frequency oscillation, ~7 MHZ, is associated with the "ringout" circuit components described above. The discharges occur at the large negative peak on the current waveform (approximately 5 ns wide). The subsequent fast oscillations are the result of the voltage collapse across the air gap when the micro discharges occur and the decay of the associated resonant energy stored locally in the

low inductance cell geometry. Only a small percentage, 2% to 4%, of the energy stored in C_s is dissipated in the discharge. This can be understood by recognizing that only the energy stored locally in the air gap is available to the discharge, while most of the initial stored energy sent to the load is used to charge the comparatively large cable capacitance. This energy and remaining energy in C_s is dissipated in R_r to prepare the system for another negative pulse.

B. Dielectric-Barrier Discharge Cell

A small single dielectric-barrier discharge cell was constructed for use in these low power "bench-top" experiments. Figure 3 provides an illustration of the cell showing the two possible discharge modes. The nylon insulating housing has two gas ports and four window ports (not shown). The upper high-voltage electrode disk is imbedded in the housing and a Pyrex disk, which provides the single dielectric barrier, is bonded to the housing underneath the electrode. The cell could be configured in two ways, 1) a single-barrier/pin arrangement in Fig. 3a or 2) a single-barrier/flat electrode arrangement in Fig. 3b. In Fig. 3a, a 1.5 mm diameter stainless steel pin is used as the lower electrode and is surrounded by a nylon spacer to provide a flat surface at the bottom of the air gap. The advantage of this arrangement is that a micro discharge (lasting less than ten nanoseconds) is produced at the location of the pin with a low temporal jitter which makes it possible to use a short laser pulse to probe the plasma. Also the time evolution and decay of chemical species can be observed using this configuration. The disadvantage of this elec-trode arrangement is that removal efficiency measurements cannot be obtained since the plasma does not fill the whole volume. The electrode arrangement in Fig. 3b, however, can be used to measure the removal efficiency since a flat stainless steel disk is used as the lower electrode enabling the volume between the plates to be filled with micro discharges. The complete assembly, cell and electrical diagnostic probes, were mounted in an alumi-num enclosure to reduce the inductance at the cell and provide shielding. The high-voltage feedthrough connects the cable ground to the enclosure and the center conductor of the cable to the high-voltage electrode of the cell. A picture of the micro discharge in nitrogen using the barrier/pin

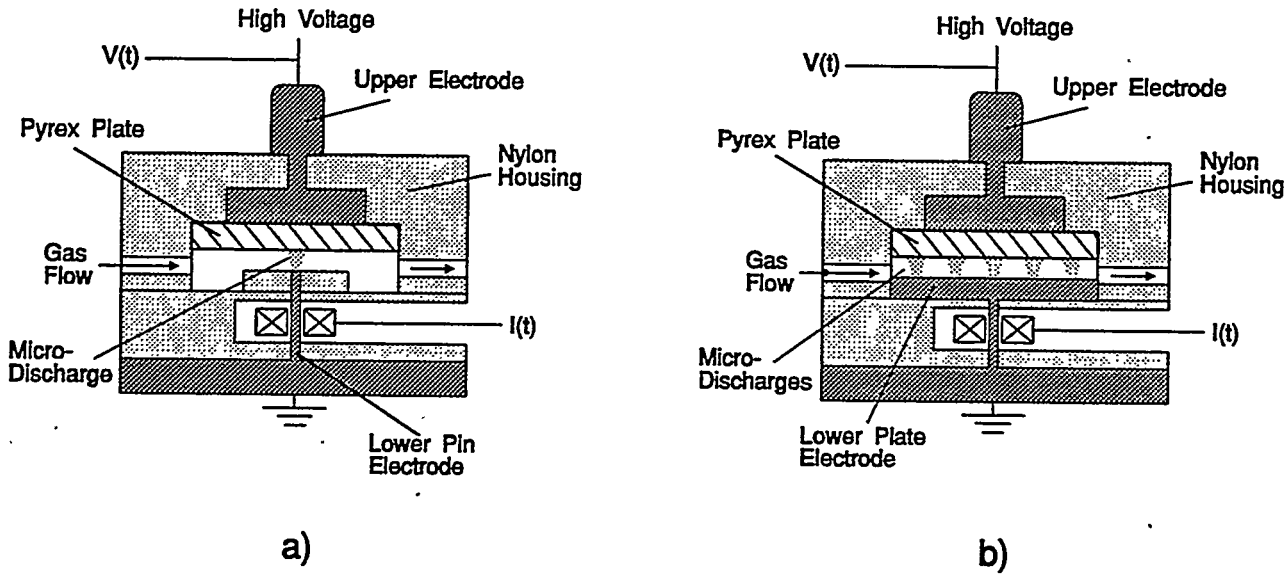

Figure 3. A diagram of the dielectric-barrier discharge cell where a) is the single-barrier/pin arrangement and b) is the single-barrier/plane electrode arrangement.

arrangement is shown in Fig. 4. In this picture the "footprint" of the region of charge extracted from the glass plate is approximately four times larger than the pin diameter.

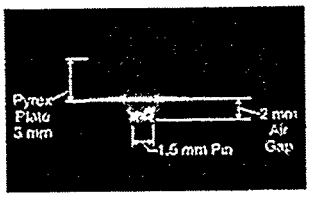

Figure 4. A photograph of the discharge produced in the single-barrier/pin arrangement in nitrogen.

C. Chemical Diagnostics

A gas bottle was filled to a high pressure with either a mixture of dry air and TCE or a mixture of NO in dry nitrogen as seen in Fig. 5. A gas regulator and mass flow controller were used to set the flow through the discharge cell before entering the vent (for TCE) or the gas bag (for NO). The method for measuring the reduction of TCE used a gas-tight syringe to extract a sample at a known volume from the gas output line which was then injected into a gas chromatograph with a sample concentrator (Varian model Star 3400CX GC and OI Corp. - model 4460A sample concentrator). To measure the reduction of NO in dry nitrogen at the low flow rates (50 mL/min) needed to achieve an energy density, E, up to 100 J/l, a gas bag was filled slowly over 40 minutes at a partic-ular energy density setting and then pumped through the chemiluminescent gas analyzer (California Analytical Instruments, model 240-CLD) at 1.5 L/min.

III. EXPERIMENTAL RESULTS

The removal efficiency of NO in nitrogen using a pulsed dielectric barrier discharge was compared to that previously obtained from a peak voltage of 30 kV [7]. The pulsed corona tube (90 cm long) was constructed using a 500 μm diameter stainless steel wire center conductor with a 2.4 cm diameter stainless steel tube as the outer conductor. The E/N at breakdown of both discharges was approximately 500 Td (at room temperature and pressure). A comparison of the removal efficiency for the two discharge types is shown in Fig. 6. The removal efficiency is close to the same between the pulsed dielectric-barrier and corona discharges indicating that the gaseous electronics occurring in the discharges and the resulting chemistry are similar.

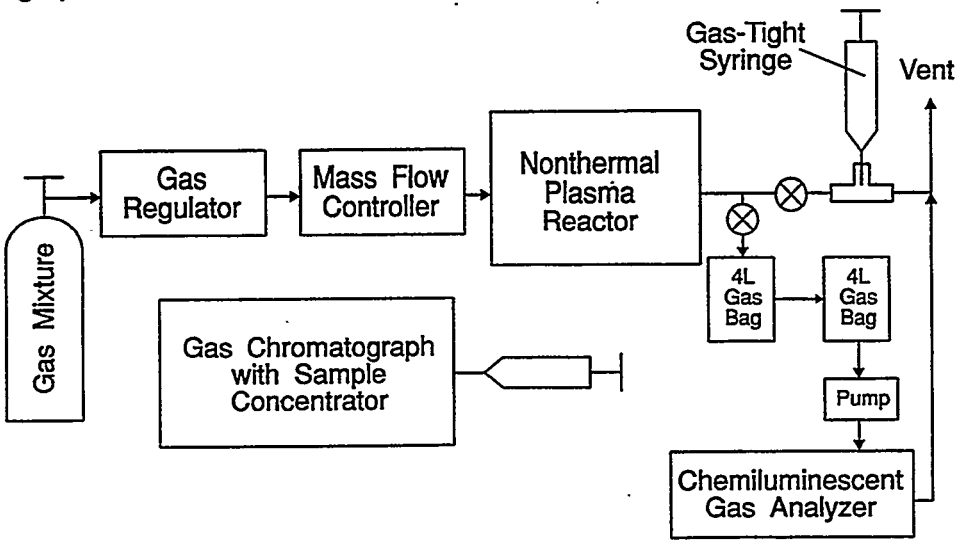

Figure 5. The chemical diagnostics setup used to obtain removal efficiency data for TCE (gas tight syringe) and for NO in Nitrogen (Teflon gas bag).

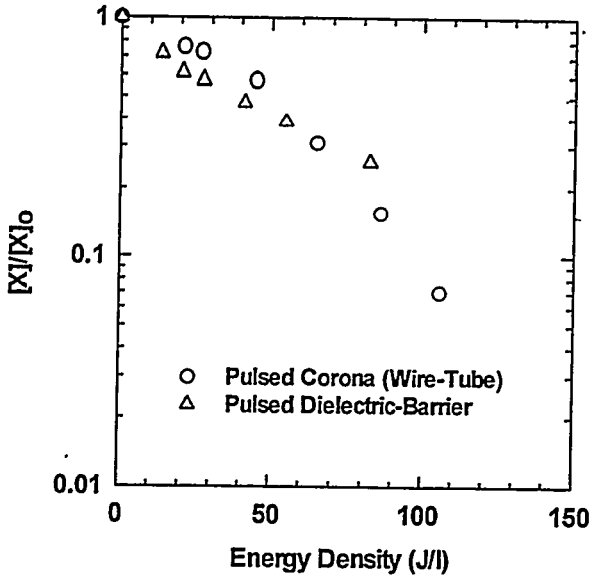

Figure 6. The removal efficiency, $[X]/[X]_o$, versus energy density for 500 ppm of NO in nitrogen using both pulsed corona and pulsed dielectric-barrier discharges.

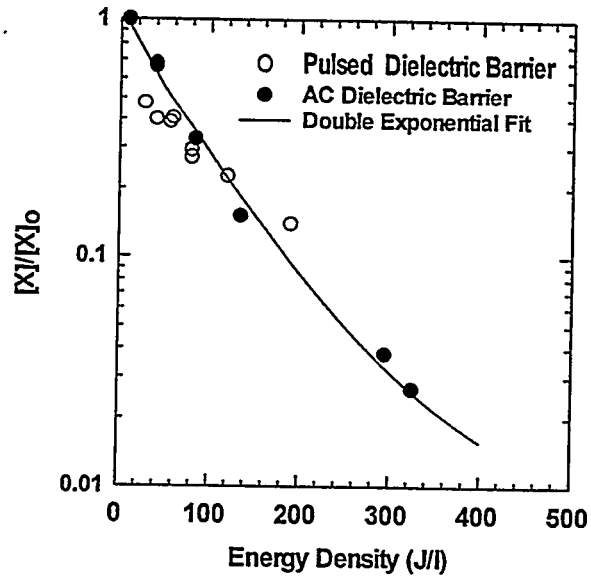

Figure 7. The removal efficiency, $[X]/[X]_o$, versus energy density for 200 ppm of TCE in dry air using both pulsed and ac-driven dielectric-barrier discharges.

The removal efficiency of TCE in dry air using a pulsed dielectric barrier discharge was compared to that previously obtained from an ac-driven dielectric-barrier discharge. The ac-driven dielectric-barrier discharge was powered by a sinusoidal power supply at a frequency of 1.2 kHz with a peak voltage of 25 kV [7]. The discharge cell was constructed in a flat-plate geometry using two 0.3 cm x 38 cm x 70 cm Pyrex plates with a gap spacing of 3.5 mm and an active discharge area of 1800 cm^2. Two aluminum electrode plates were pressed to each side of the cell with a charge measuring capacitor between the low voltage plate and ground. The E/N at breakdown of the pulsed dielectric-barrier discharge was much larger than that of the ac-driven discharge, 500 Td for the pulsed discharge and 80 Td for the ac-driven discharge. A comparison of the removal efficiency for the two discharge types is shown in Fig. 7. Even with the large difference in E/N at breakdown between the two differently-driven discharges, the removal efficiency was close to the same between the pulsed and ac-driven discharges. In this case it is known that the primary decomposition-initiating chemical reaction is between $O(^3P)$ and TCE. The results in Fig. 7 indicate that the generation of $O(^3P)$ radicals is similar between the two types of barrier discharges.

IV. SUMMARY

A small, single dielectric-barrier discharge cell driven by a fast risetime pulse generator circuit has been constructed to investigate NO_x reduction. The thyratron switched fast-pulse circuit used to drive the dielectric-barrier discharge had a risetime of 6.5 ns, a maximum peak output voltage of 40 kV, a maximum repetition rate of 20 Hz, and a temporal jitter of 4 ns. This pulsed dielectric-barrier discharge and a pulsed corona discharge were compared in terms of the removal efficiency of 500 ppm of NO in nitrogen. The removal efficiency of 200 ppm of TCE in dry air has been compared between this pulsed dielectric-barrier discharge and an ac-driven dielectric-barrier discharge.

REFERENCES

1. Non-Thermal Plasma Techniques for Pollution Control, edited by B.M. Penetrante

and S.E. Schultheis, Part A and Part B (Springer-Verlag, Berlin Heidelberg, 1993).

2. J.J. Coogan and A.D. Sappey, "Distribution of OH Within Silent Discharge Plasma Reactors, IEEE Trans. Plasma Sci., Vol. 24, No. 1, pp. 91-92, 1993.

3. D. Evans, L.A. Rosocha, G.K. Anderson, J.J. Coogan, and M.J. Kushner, Plasma Remediation of Trichloroethylene in Silent Discharge Plasmas," J. Appl. Phys., Vol. 74, No. 9, pp. 5378-5386, 1993.

4. B.M. Penetrante, M.C. Hsiao, B.T. Merritt, GE. Vogtlin, and P.H. Wallman, "Comparison of Electrical Discharge Techniques for Nonthermal Plasma Processing of NO in N2," IEEE Trans. Plasma Sci. Vol. 23, No. 4, p. 679-687, 1995.

5. P.H. Wallman, M.C. Hsiao, B.T. Merritt, B.M. Penetrante, and G.E. Vogtlin, "Nonthermal Aftertreatment of Diesel Engine Exhaust," Proceedings of the 1995 Diesel Engine Emissions Reduction Workshop, La Jolla, California, July 24-27, 1995.

6. M.J. Nusca, P.A. Sagear, andA.W. Miziolek, "Experimental and CFD Studies of Non-Thermal Plasmas for NOx Control," Proceedings of the 2nd International Symposium on Non-Thermal Plasma Technology for Pollution Control, Salvador, Brazil, August 11-15, 1997.

7, R.A. Korzekwa and L.A. Rosocha, "Experimental Results Comparing Pulsed Corona and Dielectric Barrier Discharges for Pollution Control," Presented at the 11th IEEE International Pulsed Power Conference, Baltimore, Maryland, June 29 - July 2, 1997.